Cellular cholesterol abundance regulates potassium accumulation within endosomes and is an important determinant in bunyavirus entry

Frank W. Charlton[‡], **Samantha Hover**[‡], **Jack Fuller**[§], **Roger Hewson**[§], **Juan Fontana**[‡¶1], **John N. Barr**[‡¶2], and **Jamel Mankouri**[‡¶3]

From the [‡]*School of Molecular and Cellular Biology and* [¶]*Astbury Centre for Structural Molecular Biology, University of Leeds, Leeds LS2 9JT, United Kingdom and the* [§]*National Infection Service, Public Health England, Porton Down, Salisbury SP4 0JG, United Kingdom*

Edited by Charles E. Samuel

The Bunyavirales order of segmented negative-sense RNA viruses includes more than 500 isolates that infect insects, animals, and plants and are often associated with severe and fatal disease in humans. To multiply and cause disease, bunyaviruses must translocate their genomes from outside the cell into the cytosol, achieved by transit through the endocytic network. We have previously shown that the model bunyaviruses Bunyamwera virus (BUNV) and Hazara virus (HAZV) exploit the changing potassium concentration ($[K^+]$) of maturing endosomes to release their genomes at the appropriate endosomal location. K^+ was identified as a biochemical cue to activate the viral fusion machinery, promoting fusion between viral and cellular membranes, consequently permitting genome release. In this study, we further define the biochemical prerequisites for BUNV and HAZV entry and their K^+ dependence. Using drug-mediated cholesterol extraction along with viral entry and K^+ uptake assays, we report three major findings: BUNV and HAZV require cellular cholesterol during endosomal escape; cholesterol depletion from host cells impairs K^+ accumulation in maturing endosomes, revealing new insights into endosomal K^+ homeostasis; and "priming" BUNV and HAZV virions with K^+ before infection alleviates their cholesterol requirement. Taken together, our findings suggest a model in which cholesterol abundance influences endosomal K^+ levels and, consequently, the efficiency of bunyavirus infection. The ability to inhibit bunyaviruses with existing cholesterol-lowering drugs may offer new options for future antiviral interventions for pathogenic bunyaviruses.

The order Bunyavirales represents the largest taxonomic collection of single-stranded, negative-sense RNA viruses, with over 500 named isolates classified into 10 families and 35 genera (1).[4]

Bunyaviruses infect a wide range of hosts, including animals, plants, insects, and humans. Viruses able to infect humans are classified into just four of the Bunyavirales families, Hantaviridae, Phenuiviridae, Nairoviridae, and Peribunyaviridae, with selected species able to cause potentially fatal hemorrhagic fever or encephalitis in their human hosts (2).

The genome of all bunyaviruses comprises three linear RNA segments that are named according to their relative size, with the large (L)[5] segment encoding the viral RdRp, the medium (M) segment encoding envelope-associated glycoproteins (G_n and G_c) and the small (S) segment encoding the nucleoprotein (N), which encapsidates the RNA segments to form ribonucleoprotein (RNP) complexes. In many bunyavirus species, an additional nonstructural protein (NSs) is expressed from the S segment either from an overlapping ORF on the N mRNA or, alternatively, via generation of a discrete mRNA through ambisense transcription (3). Many bunyaviruses also express a nonstructural protein from the M segment (NSm), which is cleaved from the single polyprotein precursor transcribed from the single M segment mRNA (4–6).

For bunyaviruses to establish infection, they must penetrate host cells and traverse the endocytic network prior to escape of viral RNPs into the cytosol and subsequent gene expression. Cell penetration of bunyaviruses occurs through attachment of the virus to the cell, followed by internalization through a range of mechanisms. It is known that viruses of the families Hantaviridae, Nairoviridae, and Peribunyaviridae are endocytosed through a clathrin-dependent mechanism, with functional roles for caveolar endocytosis and macropinocytosis also described. Conversely, viruses of the Phenuiviridae enter cells independently of clathrin (7–10). When inside endosomes, bunyaviruses must facilitate the escape of their RNPs into the cytosol, a process involving fusion of the virus envelope with the endosomal membrane. This fusion event is mediated by the heteromultimeric glycoprotein spikes comprising G_n and G_c, arranged on the surface of mature virions

in a variety of different architectures (11–14). For the fusion machinery to be activated, the glycoprotein spikes must be subjected to a variety of specific biochemical events that can occur before or after their inclusion in the virion. For instance, most class I and II fusion proteins studied to date require a proteolytic cleavage event to become fusion-competent (15). This event is termed "priming," after which a variety of further events, known as "triggers," induce structural changes in the fusion proteins, resulting in a transition between pre- and post-fusion conformations. Although the priming step involves proteolysis, there is a greater variety of triggers, including pH and interactions with an internal or external cellular receptor. These triggering events ensure that fusion between viral and cellular membranes is restricted to an appropriate cellular location that leads to productive infection (15).

Recently, we used the prototypic bunyavirus Bunyamwera virus (BUNV) and the model nairovirus Hazara virus (HAZV) to reveal that bunyavirus fusion depends on specific changes in both pH and ion balance (16, 17). Specifically, we identified K$^+$ as a critical biochemical trigger required for spike conformational changes and interaction with membranes, consistent with activation of the fusogenic machinery. Although this work documented how bunyavirus glycoproteins respond to specific endosomal conditions, it is likely that efficient fusion between virus and endosomal membranes requires other biochemical factors, such as specific vesicle lipid environments and/or endosomal receptors. In this regard, it is known that the composition of biological membranes is crucial for the physiological function of cells and that cholesterol is an important regulator of membrane integrity and fluidity, making up 25–50% of the total lipid content of animal cells (18). Aberrations in cholesterol homeostasis can disrupt cellular uptake mechanisms, which is important from the view of enveloped viruses. The correct composition of biological membranes in terms of cholesterol has been shown to be important to the life cycle of several enveloped viruses, in a variety of life cycle stages ranging from entry to release. As well as the correct environmental pH, the Togaviridae family member Semliki Forest virus requires high cholesterol composition in target membranes for stable insertion of its fusion loop (19), whereas the hantavirus Andes virus (ANDV) has been demonstrated to require high cholesterol in target membranes for productive infection (20). Cholesterol concentrations also influence the hemifusion stage of influenza virus fusion (21). Aside from the entry stages of viral life cycles, cholesterol has been shown to be important in the assembly and release of mature influenza virus virions, which require cholesterol to stabilize virions prior to release (22).

In this study, we examined how the biochemical composition of both host and viral membranes influences the crucial fusion step in the bunyavirus life cycle. We reveal new insights into the role of cholesterol during virion endocytic trafficking and endosomal K$^+$ accumulation.

Results

BUNV infection is inhibited by cellular cholesterol depletion

Given that enveloped viruses must fuse their outer membranes with host membranes to cause infection (23), we first examined whether cholesterol, a key regulator of membrane fluidity (24), has a role in this process. Cholesterol-rich microdomains within the plasma membrane are important for the life cycle of a range of enveloped viruses, but their role during the bunyavirus life cycle is poorly characterized.

In the following experiments, cellular cholesterol was extracted from the plasma membrane of BUNV-susceptible A549 cells using methyl-β-cyclodextrin (MβCD), and its influence on BUNV infection was assessed (Fig. 1). Cells were treated with MβCD for 45 min to sequester cellular cholesterol and incubated with BUNV (m.o.i. 0.2) for 2 h to permit virus penetration. Noninternalized viruses were removed 2 h post-infection (hpi) through trypsin washing, and the ability of BUNV to establish an infection after 24 h was assessed through detection of BUNV-N by immunofluorescence staining (Fig. 1, *A* and *B*). Quantification of cells positive for BUNV-N revealed significantly reduced levels of infection upon MβCD treatment (reduction to ∼19%) (Fig. 1*B*, *black columns*). When BUNV infection was assessed at varying concentrations of MβCD (0.5–2 mM) by Western blotting (Fig. 1, *C* and *D*), N expression was barely detectable at 0.5–1 mM and completely undetectable at 2 mM MβCD (Fig. 1*C*), revealing a concentration-dependent decrease (Fig. 1*D*, *black columns*). Importantly, MβCD treatment was noncytotoxic, as evidenced through MTS assays (Fig. 1, *B* and *D*, *gray columns*) and the equivalent levels of GAPDH in the corresponding protein lysates (Fig. 1*C*).

To confirm the BUNV cholesterol requirement, the effects of PF-429242 (an S1P/SKI-1 inhibitor) (25) and U-18666A (a lysosomal cholesterol export inhibitor) (26), which reduce cellular cholesterol through inhibition of its production and trafficking, respectively, were assessed (Fig. 1, *E–H*). Both PF-429242 and siRNA-mediated S1P inhibition have been shown to inhibit ANDV (27), whereas U-18666A has inhibitory effects on a number of important enveloped viruses, including dengue virus, Chikungunya virus, and Ebola virus (28–30). For these experiments, cells were pretreated with PF-429242 for 24 h (31) and infected with BUNV (m.o.i. 0.2, 24 h). Ammonium chloride (NH$_4$Cl), a known inhibitor of BUNV fusion, was included in these assays as a positive control (16). PF-429242 at 20 μM resulted in almost complete abrogation of BUNV-N production, whereas 5–10 μM led to drastically reduced BUNV-N expression (Fig. 1*E*). Quantification revealed that the BUNV-N levels decreased to 7.91%, 17.54%, and 37.94% in 20, 10, and 5 μM drug-treated cells, respectively, compared with the no-drug control (Fig. 1*F*, *black columns*). MTS assays revealed no detrimental effects of PF-429242 on cell viability (Fig. 1*F*, *gray columns*).

For further confirmation, cells were treated with U-18666A under identical conditions (26). Fig. 1*G* shows strong inhibition of BUNV in cells treated with 5–10 μM U-18666A and more modest inhibition at 2.5 μM U-18666A. Upon quantification (Fig. 1*H*, *black columns*), BUNV-N expression was reduced to 8.52%, 22.83%, and 42.66% by 10, 5, and 2.5 μM U18666A, respectively. MTS assays confirmed no loss of viability at the U18666A concentrations assessed (Fig. 1*H*, *gray columns*).

Finally, we assessed cholesterol depletion as a viable anti-BUNV strategy through assessment of the inhibitory effects of the clinically approved cholesterol-lowering drug simvastatin. Fig. 1, *I* and *J*, shows that BUNV-N expression was reduced by
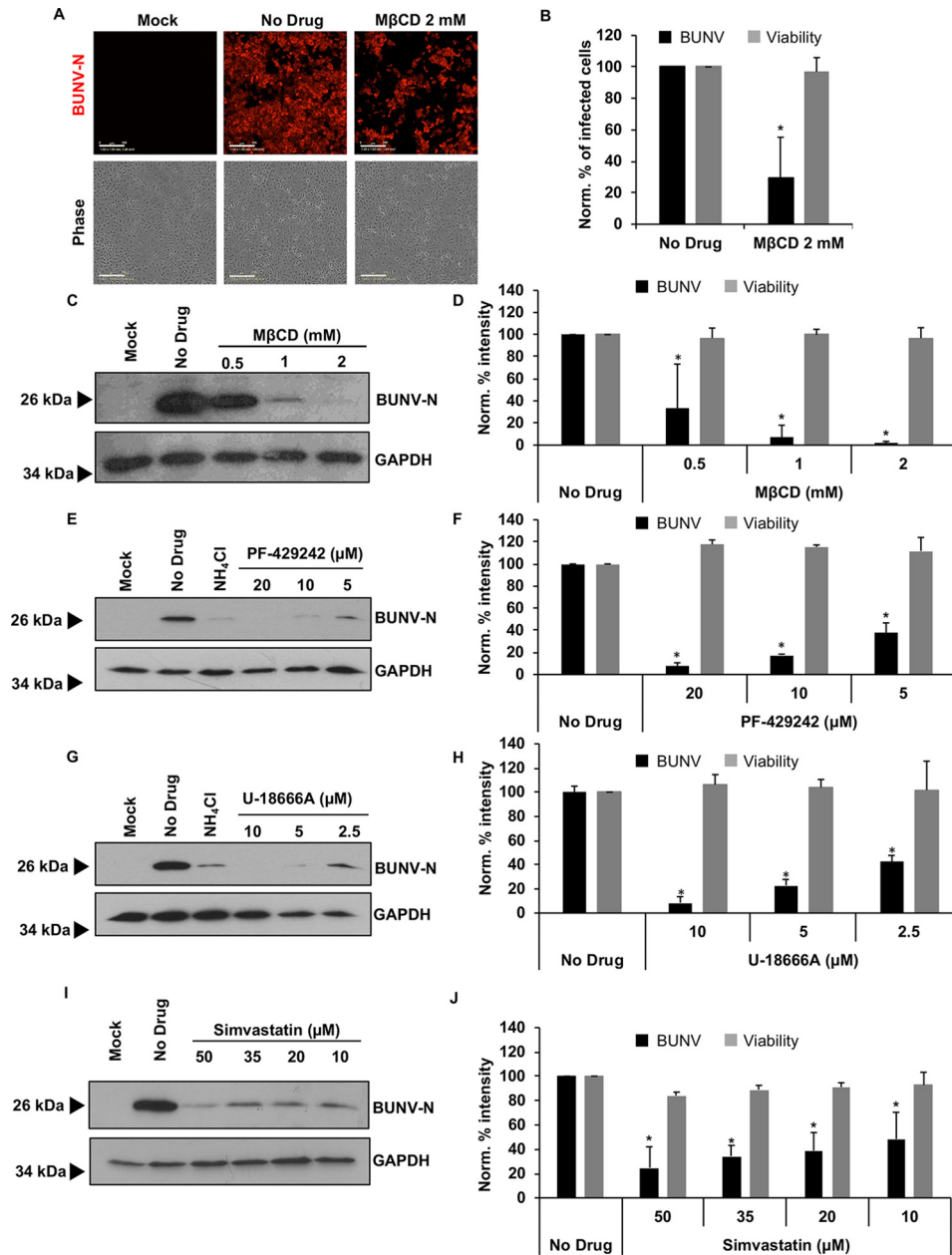
Figure 1. BUNV infection is inhibited by cellular cholesterol depletion. *A*, A549 cells were treated with MβCD for 45 min and infected with BUNV (m.o.i. 0.2). At 24 hpi, cells were fixed and stained for BUNV-N. Wide-field images were taken using an IncuCyte ZOOM® (representative images are shown). *Scale bars* = 200 μm. *B*, the percentage of BUNV-infected cells was quantified using IncuCyte Zoom® software and normalized to no-drug cells (*black columns*). *, $p < 0.05$; *error bars* are representative of $\pm$ S.D.; $n = 3$). Cell viability was assessed by MTS assays. Values were normalized to no-drug cells (gray *columns*). *C*, entry assays were performed as in *A*, cell lysates were resolved via SDS-PAGE, and BUNV-N expression was assessed by Western blot analysis. GAPDH was probed as a loading control. *D*, densitometry analysis of *C*. Band densities were normalized to no-drug BUNV–infected cells (*black columns*). MTS cell viability data are also shown (*gray columns*). *, $p < 0.05$. *E*, BUNV entry assays were performed in the presence of PF-429242. Cells were treated with 5–20 μM PF-429242 for 24 h and infected with BUNV (m.o.i. 0.2) for a further 24 h. Cells were lysed, and lysates were resolved via SDS-PAGE and screened for BUNV-N and GAPDH. *F*, densitometry analysis of *E*. *, $p < 0.05$. *G*, entry assays were performed as in *E*, with U-18666A at 2.5–10 μM. *, $p < 0.05$. *H*, densitometry analysis of BUNV-N expression following U-18666A treatment. *, $p < 0.05$. *I*, entry assays as in *E*, with 10–50 μM simvastatin. *J*, densitometry analysis of *I* as in *D*. *, $p < 0.05$.

50, 35, 20, and 10 μM simvastatin treatment to 24.74%, 34.29%, 38.82%, and 48.37%, respectively, when normalized to no-drug controls. MTS assays confirmed no drug-induced cytotoxicity (Fig. 1*J*, *gray columns*). Taken together, these data, obtained via four independent methods, strongly suggest that cholesterol is important during the BUNV life cycle and that clinically approved cholesterol-lowering drugs hold promise as a clinically available antiviral strategy.

Both the virion envelope and cellular cholesterol influence BUNV infection

As BUNV is an enveloped virus, we next assessed whether envelope cholesterol contributed to the effects of cholesterol-lowering compounds. To assess this, we used a recombinant BUNV containing GFP inserted at the N terminus of a truncated G$_c$ glycoprotein (GFP-G$_c$) with the deleted sequence shown to be dispensable for virus infection in cell culture (32,
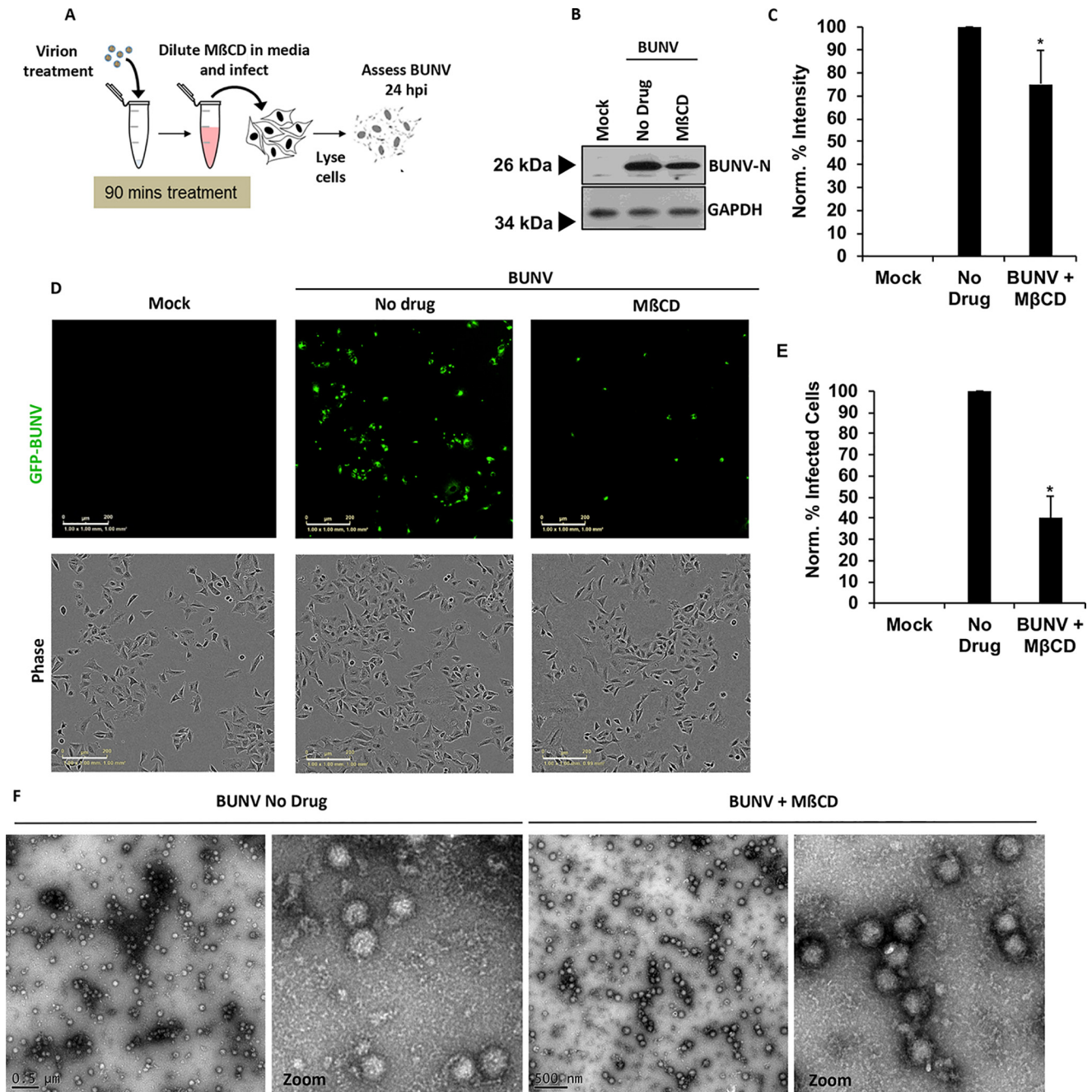
Figure 2. BUNV envelope cholesterol is also required for virus infection. *A*, schematic of BUNV envelope cholesterol extraction. GFP-BUNV virions were treated with MβCD for 90 min, and the drug/virus was diluted in DMEM and added to A549 cells for 24 h (m.o.i. 0.5). *B*, cells were lysed, and BUNV-N expression was assessed by Western blot analysis. *C*, blots were quantified by densitometry analysis and normalized to no-drug controls (*, $p < 0.05$; *error bars* ± S.D.; $n = 3$). *D*, virions were treated as in *A*, and GFP expression, as a marker of BUNV infection, was assessed by IncuCyte analysis. Representative wide-field images are shown. *Scale bars* = 200 μm. *E*, percentage of cells infected by MβCD-treated virions were measured using IncuCyte Zoom® software (*, $p < 0.05$; *error bars* ± S.D.; $n = 3$). *F*, purified BUNV virions were treated with 2 mM MβCD for 90 min at 37 °C. Treated and untreated (no-drug) virions were loaded onto carbon-coated grids and negatively stained with 1% uranyl acetate. Images were taken at 120 kV on a Tecnai T12 electron microscope. *Scale bars* = 0.5 μm.

33). GFP-BUNV virions were treated *in vitro* with MβCD for 90 min at 37 °C to sequester cholesterol from the virion membrane (Fig. 2*A*). To mitigate the effects of MβCD on the cells, virions were diluted in medium prior to infection (m.o.i. 0.5, 24 h). This ensured that any effects of cholesterol depletion were mediated by direct effects on the virions as opposed to cellular effects.

From these experiments, we observed a ∼25% decrease in total BUNV-N expression following direct MβCD virion

treatment (Fig. 2, *B* and *C*) by Western blot analysis. Upon assessment of GFP-G$_c$ fluorescence (32) (Fig. 2*D*), a larger, ∼60% decrease in the number of infected cells was observed (Fig. 2*E*). This confirmed that MβCD virion treatment decreased the number of infected cells. The ultrastructure of BUNV virions was unaffected by cholesterol depletion, as negative staining showed no gross structural defects in the virions following MβCD treatment (Fig. 2*F*). We therefore

reasoned that BUNV infection depends on virion as well as cellular associated cholesterol.

Cellular cholesterol depletion influences BUNV endocytic escape but not cell penetration

To further dissect the role of cholesterol during BUNV infection and identify the steps at which MβCD-mediated cholesterol extraction inhibits the virus life cycle, time-of-addition assays were performed. We included NH_4Cl as a control, an endosomal acidification inhibitor that inhibits BUNV at early stages of infection, *i.e.* only during its movement through the endocytic system (16). Cells were infected with BUNV (m.o.i. 0.2, $t = 0$), and NH_4Cl or MβCD was added to cells at defined time points up to and including 10 hpi. Infection was then allowed to proceed until 24 hpi, and BUNV-N expression was assessed (Fig. 3, *A* and *B*). Fig. 3, *A* and *C*, shows that BUNV escapes from endosomes at or before 6 hpi, as NH_4Cl treatment did not influence BUNV-N production when added at 6 hpi or later, consistent with our previous findings (16). Interestingly, BUNV sensitivity to MβCD followed a similar time course (loss of inhibition from 6–8 hpi; Fig. 3, *B* and *C*), suggesting that MβCD also inhibits BUNV early stages of infection. Next, using tris(2-carboxyethyl)phosphine (TCEP) to distinguish internalized and surface-bound particles, we assessed the kinetics of BUNV cell penetration. TCEP is a membrane-impermeable reducing agent that inactivates BUNV exposed extracellularly or at the plasma membrane. We observed loss of TCEP inhibition when added 40 min post-virus addition, as assessed by immunofluorescence (Fig. 4, *D* and *E*) and Western blot analysis (Fig. 4*F*). Taking into account the NH_4Cl effects on BUNV, this confirmed that BUNV is resident in the endosomal system from 40 min to 6 h post-infection. Importantly, an effect of cholesterol depletion on BUNV cell penetration was discounted, as we observed fluorescently labeled BUNV (BUNV-DiDvbt/SYTO82), in which the viral envelope was labeled with DiDvbt and its RNA genome was labeled with SYTO82 in distinct endosomal puncta in cells treated with MβCD, suggesting that BUNV can penetrate cells depleted of cholesterol (Fig. 3, *D* and *E*). These data suggest that the critical role of cholesterol in the BUNV life cycle occurs at a post-penetration ($\geq$40 min) endocytic stage ($\leq$6 h), in agreement with that observed for other enveloped viruses (35).

Cholesterol extraction reduces K⁺ accumulation in endosomes

We recently demonstrated that an increasing K⁺ gradient is required to induce a fusogenic state in BUNV and HAZV as they traffic through the endocytic network (16, 36), with high [K⁺] acting as a biochemical cue for priming/activation of the fusion glycoproteins G_n/G_c (17). Blocking K⁺ influx into endosomes was shown to trap virions in the endocytic system, after which they accumulated in lysosomes for subsequent degradation.

Based on this knowledge and our observation that cholesterol depletion influences BUNV at the stage of endosomal trafficking, we explored whether cholesterol depletion also influences endosomal K⁺ accumulation. To test this, we used the K⁺-sensitive, membrane-impermeable fluorescent dye Asante-K⁺ green 4 (AG4), which specifically labels endosomal

K⁺. Endosomes rich in K⁺ could be observed within cells, where the intensity of the AG4 signal indicates the degree of K⁺ accumulation (Fig. 4, *A* and *B*). When cells were treated with MβCD for 45 min and AG4 was added, the number of AG4 puncta was reduced compared with untreated cells (Fig. 4, *A* and *B*), suggesting that cholesterol depletion reduces the number of K⁺-rich endosomes. Alexa Fluor 594®– conjugated transferrin (TF-594) was used as a control in these experiments to demonstrate no interference of MβCD with general fluorescence or cellular uptake pathways (Fig. 4, *A* and *C*). Interestingly, we found that the intensity of TF-594 increased in MβCD-treated cells (2-fold increase), which may be attributed to a shift between recycling and degradation pathways following cholesterol depletion. The above data were confirmed through quantification of the AG4 and TF-594 signals (Fig. 4, *B* and *C*, respectively), where the AG4 signal was reduced to 41.6% and TF-594 increased by 81.6% following MβCD treatment. These data reveal an important cell biological phenomenon whereby endosomal K⁺ accumulation depends on cholesterol within endosomal membranes.

To further dissect the relationship between endosomal K⁺ and cholesterol, we primed BUNV virions for fusion by incubation with K⁺ prior to their addition to cells depleted of cholesterol. K⁺ priming leads to activation of the viral fusion machinery so that endosomal K⁺ concentrations no longer influence fusion. If the inhibitory effect of MβCD on infection is a consequence of altering K⁺ within endosomes, then this K⁺ priming should alleviate the effect of MβCD on virus growth.

To test this, cells were treated with MβCD for 1 h, whereas virions were incubated for 2 h in mildly acidic buffers (pH 6.35) with or without exposure to high K⁺. Following incubation, the virions were incubated in normal medium prior to infection (m.o.i. 0.1) to dilute out the high K⁺ and return the pH to neutral. Infection was allowed to proceed for 18 h to allow initiation of BUNV-N production according to our previous time course analysis (17).

The data in Fig. 4*D* show a significant increase in BUNV-N production when virions are treated in the presence of K⁺ (+), compared with without K⁺ (−), consistent with our previous studies demonstrating that pH 6.35/K⁺ primed virions undergo an accelerated entry stage of their life cycle (16). In cells treated with MβCD, infection was notably decreased for virions incubated without high K⁺, consistent with that shown in Fig. 1. Critically however, when virions were treated with pH 6.35/high K⁺, infection in the presence of MβCD treatment was almost equivalent to no-drug cells, suggesting that K⁺ primed virions overcome the effects of MβCD and thus do not require cellular cholesterol (Fig. 4, *D* and *E*). The activity of MβCD in these assays was further confirmed through its known ability to inhibit epidermal growth factor uptake (Fig. 4*F*). Taken together, these data imply that the major effects of cholesterol depletion on BUNV are mediated through its effects on cellular endosomal [K⁺].

Cellular cholesterol is also required for HAZV infection through its effects on endosomal K⁺

BUNV and HAZV are both members of the Bunyavirales order, and their entry pathways have similarities (6, 32, 33). We

SASBMB

J. Biol. Chem. (2019) 294(18) 7335–7347 **7339**

therefore examined whether HAZV, like BUNV, requires cellular cholesterol during entry, thus establishing the possibility of an order-wide dependence.

We first explored whether cholesterol depletion similarly impedes HAZV infection using experimental conditions identical to those described for BUNV. Cells were infected with
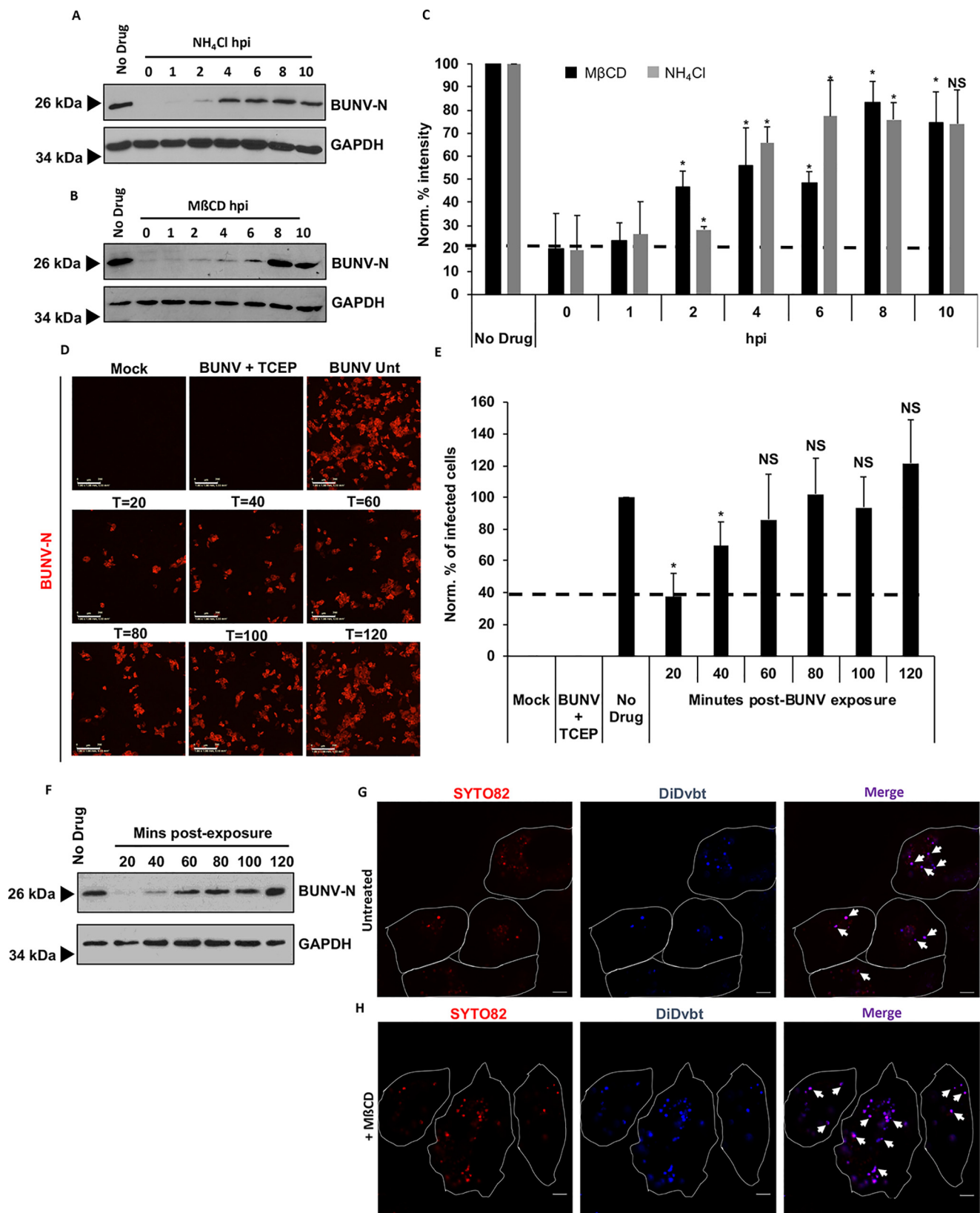
HAZV (m.o.i. 0.2), and the reliance on cholesterol was examined through detection of HAZV-N by either immunofluorescence or Western blotting. Following cellular MβCD treatment, a clear decrease in the number of HAZV-infected cells was observed (Fig. 5A), which, when quantified, revealed a 59.47% decrease compared with no-drug controls (Fig. 5B, *black columns*). These data were supported by a Western blot analysis (Fig. 5C) in which HAZV-N expression decreased in a concentration-dependent manner with 2 mM MβCD treatment, reducing HAZV-N to 78.58% (Fig. 5D). The cholesterol requirement of HAZV was further confirmed via treatment of cells with PF-429242 (Fig. 5, E and F) and U-18666A (Fig. 5, G and H). Western blot analysis of HAZV-N in PF-429242–treated cells (Fig. 5E) revealed a concentration-dependent inhibition that, when quantitated, showed a decrease in infection to 51.72%, 67.12%, and 98.66% in cells treated with 20, 10, and 5 μM PF-429242, respectively (Fig. 5F, *black columns*). When experiments were performed using U18666A, concentration-dependent inhibition of HAZV was also observed (Fig. 5G), revealing a reduction of HAZV infection to 22.98% in cells treated with 10 μM U18666A, to 35.41% with 5 μM, and to 47.52% with 2.5 μM (Fig. 5H). MTS data (Fig. 5, B, D, F, H, J, and L, *gray columns*) demonstrated no cellular toxicity in response to any drug treatment. We further sought to explore the effect of the cholesterol requirement of HAZV by using the clinically approved compound simvastatin. Western blot analysis of HAZV-N in simvastatin-treated cells revealed a concentration-dependent inhibition of infection (Fig. 5I) that, when quantified, yielded a reduction of HAZV-N to 44.77%, 59.99%, 67.64%, and 85.20% in cells treated with 50, 35, 20, and 10 μM, respectively.

We have shown previously that high [K$^+$] activates the fusion machinery of HAZV at pH 7.35 (15). Therefore, we sought to explore whether the effect of HAZV priming could also desensitize virions to the effects of cholesterol depletion. To test this, cells were treated with MβCD for 1 h, and HAZV virions were incubated for 2 h in buffers of pH 7.35 with or without high [K$^+$]. Virions were subsequently added to normal medium to highly dilute the [K$^+$] and added to cells for 18 h (m.o.i. 0.1).

Fig. 5L shows a significant increase in HAZV-N production when primed with high [K$^+$] (+) at pH 7.35 compared with unprimed virions at pH 7.35 alone (−), suggesting that these conditions expedite an early stage of the HAZV life cycle in a manner comparable with the effect seen in BUNV. Similar to the effects shown in Fig. 4, A–D, MβCD treatment significantly inhibited HAZV infection when treated without high K$^+$ (−). Importantly, when HAZV virions were primed with high K$^+$

(+), infection of MβCD-treated cells occurred at levels similar to that of no-drug cells, suggesting that HAZV is also able to overcome the effects of MβCD on cells when primed with high K$^+$. These data reinforce the dependence of HAZV on the correct endosomal environment for entry and further suggest that cholesterol mediates the formation of K$^+$-rich endosomes required for the escape of BUNV and HAZV virions.

Discussion

The composition of biological membranes is crucial for the physiological function of cells, and cholesterol is an important regulator of membrane integrity and fluidity (18). Therefore, aberrations in cholesterol homeostasis can disrupt cellular uptake mechanisms, including uptake of both beneficial and detrimental cargos.

By performing pharmacological manipulation of cellular cholesterol content via extraction with MβCD or interfering with sterol synthesis/trafficking pathways (inhibition using PF-429242, U-18666A, and simvastatin), we showed that both BUNV and HAZV are sensitive to changes in cellular cholesterol content (Figs. 1 and 5). Therefore, the peribunyaviruses and nairoviruses can be added to the list of virus families that are known to require cholesterol to establish an infection (37). This list includes many enveloped viruses, for which cholesterol depletion has been reported to disrupt specific stages of the virus life cycle. For example, in the case of the togavirus Semliki Forest virus and influenza virus, cholesterol has a role in membrane fusion (19, 35), whereas the polyomavirus SV40 requires cholesterol as it enters cells through caveola-mediated endocytosis (originating from cholesterol-rich lipid rafts) (38, 39). In the case of the flavivirus West Nile virus, cellular cholesterol depletion restricts virus replication as a result of the disruption of cholesterol-rich microdomains (40). The flavivirus hepatitis C virus is also sensitive to changes in cellular cholesterol accumulation (resulting from U-18666A treatment) but the affected stage of the replication cycle is late; namely, virus assembly and egress (31). In this study, time-of-addition experiments and the progression of labeled viruses showed that the effect of cholesterol depletion on BUNV was not at the initial stage of cell penetration but occurred during the time period when the virus escapes from the endocytic pathway. Furthermore, we showed that cholesterol depletion reduced K$^+$ accumulation in the endocytic network, leading us to question whether the role of cholesterol in BUNV entry was linked to endosomal K$^+$ homeostasis, a factor we have shown to be critical for BUNV and HAZV entry (17, 36, 41).

Figure 3. MβCD inhibits BUNV at an early post-penetration stage of infection. *A*, A549 cells were infected with BUNV (m.o.i. 0.1, *t* = 0). NH$_4$Cl was added at the indicated time points and screened for BUNV-N expression at 24 hpi by Western blotting as in Fig. 1. *B*, cells were infected and treated with MβCD as in *A*. *C*, densitometry analysis of the NH$_4$Cl and MβCD time courses in *A* and *B* (*gray* and *black columns*, respectively). Band densities were normalized to no-drug–infected cells (*, *p* < 0.05; *NS*, nonsignificant; *error bars* ± S.D.; *n* = 3). BUNV internalization takes up to 40 min. *D*, BUNV virions were added to A549 cells (m.o.i. 0.2, *t* = 0), which were treated with the cell-impermeable reducing agent TCEP for 5 min at the indicated post-infection time points (20–120 min). Cells were fixed at 24 hpi and stained for BUNV-N, and wide-field images were taken using the IncuCyte Zoom®. *Scale bars* = 200 μm. *E*, the percentage of infected cells was quantified using the IncuCyte Zoom® software. Values were normalized to no-drug infected cells (*, *p* < 0.05; *error bars* ± S.D.; *n* = 3). *F*, TCEP assays were performed as in *D*, and cell lysates were harvested and resolved via SDS-PAGE. Lysates were screened for BUNV-N by Western blot analysis. GAPDH was probed as a loading control. *G*, no-drug–treated A549 cells were infected with SYTO82/DiD-BUNV (m.o.i. ~8) for 8 h at 37 °C. Cytopainter was added 30 min prior to live imaging as a cell marker. *Scale bars* = 10 μm. Fluorescent BUNV stained with SYTO82 (emission$_{max}$ 560 nm) and DiDvbt (emission$_{max}$ 665 nm) was imaged alongside Cytopainter (emission$_{max}$ 488 nm). *H*, cells were pretreated with MβCD for 45 min prior to infection with SYTO82/DiD-BUNV and imaged as in *G*. Representative confocal images are shown (*scale bars* = 10 μm).
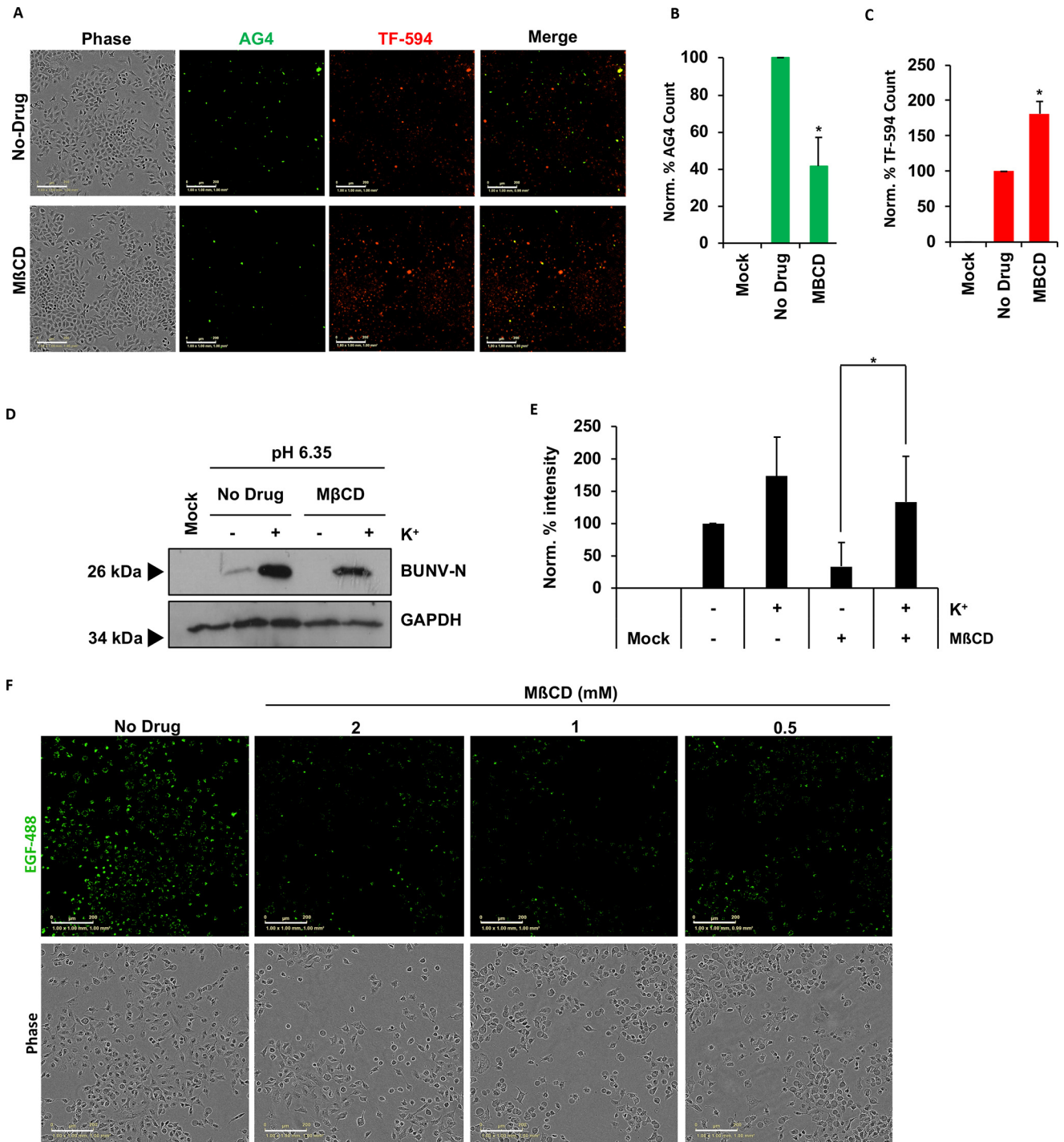
Figure 4. MβCD inhibits endosomal K⁺ accumulation, whereas K⁺-primed BUNV virions can overcome cellular cholesterol depletion. *A*, cells were pretreated with MβCD (or no-drug control) for 45 min, and the cell-impermeable K⁺ dye AG4 and TF-594 were added for 45 min at 37 °C to permit endosomal uptake. Noninternalized dyes were removed through PBS washes, and live cells were imaged using the IncuCyte Zoom®. Representative wide-field images are shown. *Scale bars* = 200 μm. *B*, AG4 fluorescence was quantified in MβCD-treated cells and normalized to no-drug cells (*, $p < 0.05$; *NS*, nonsignificant; *error bars* ± S.D.; $n = 3$). *C*, quantitative analysis of TF-594 internalization in no-drug– *versus* MβCD-treated cells, analyzed as in *B*. *D*, cells were pretreated with MβCD for 1 h, and BUNV virions were treated with buffers at pH 6.35, with or without 140 mM KCl, for 2 h at 37 °C. Buffers were diluted into 2 ml of fresh DMEM and immediately added to A549 cells. Cells were lysed at 18 hpi and immunoblotted for BUNV-N as in Fig. 1*C*. *E*, densitometry analysis of *D* as in Fig. 1*D*. *F*, cells were pretreated with 0.5, 1 or 2 mM MβCD for 45 min, and 2 μg/ml EGF-488 was added to cells for 30 min. Wide-field images were taken using IncuCyte Zoom® software. *Scale bars* = 200 μm.

However, a competing possibility was that cholesterol depletion influences membrane fluidity and thus obstructed fusion between viral and endosomal envelopes. To rule out this latter possibility, we primed BUNV by addition of K⁺, thus circumventing the need for elevated K⁺ in endosomes. Our observation that the entry of primed virus was no longer hindered by cholesterol depletion indicated that restriction of virus growth was not related to membrane fluidity. Instead, we suggest that
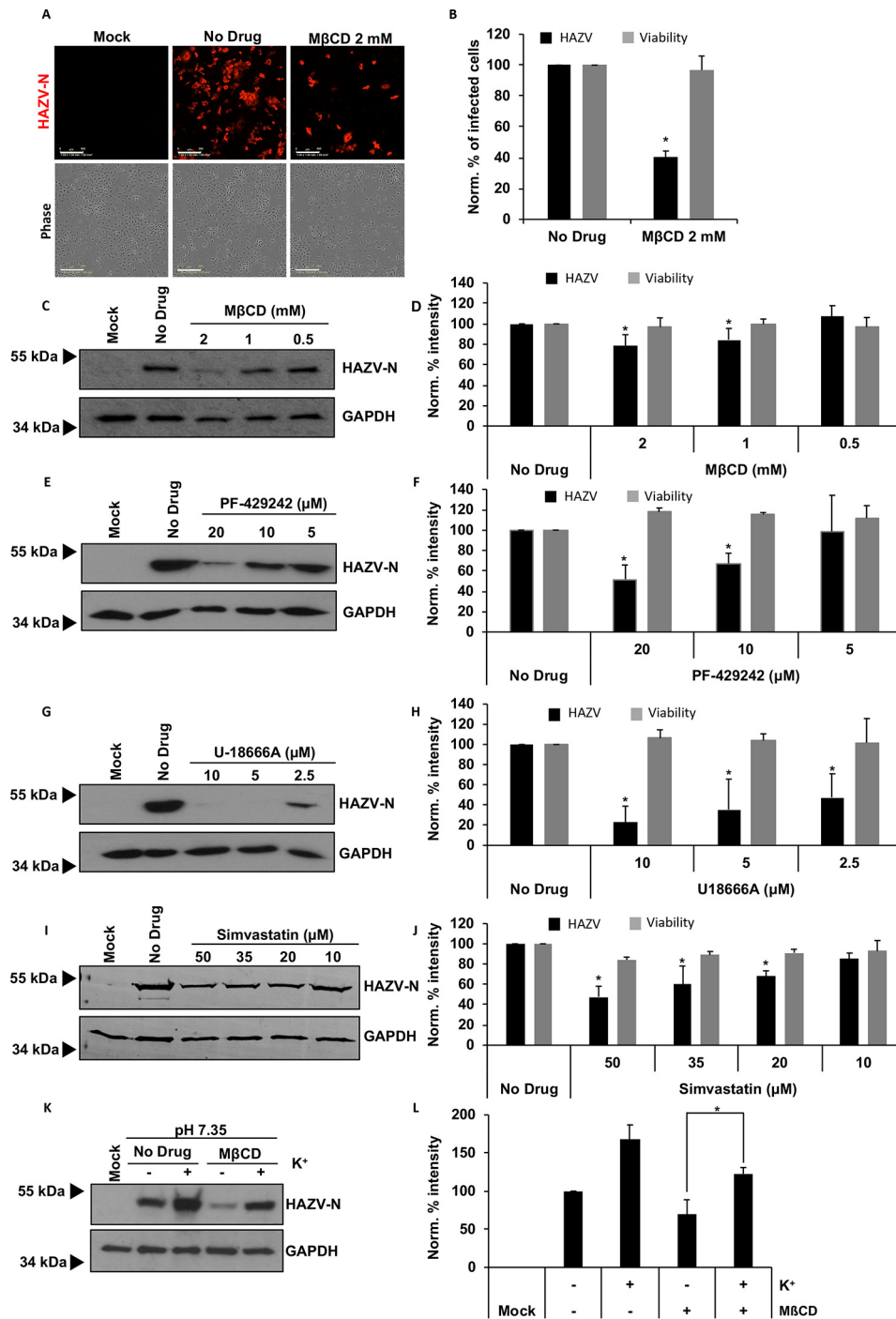
Figure 5. HAZV infection is also inhibited by cellular cholesterol depletion. *A*, A549 cells were treated with MβCD for 45 min and infected with HAZV (m.o.i. 0.2). Cells were fixed at 24 hpi and stained for HAZV-N. Wide-field images were obtained using the IncuCyte Zoom®. *Scale bars* are 200 μm. *B*, the percentage of infected cells was quantified using IncuCyte Zoom® software and normalized to no-drug cells (*black columns*; *, $p < 0.05$; *error bars* ± S.D.; $n = 3$). Cell viability was assessed by MTS assay and normalized to no-drug cells (*gray columns*). *C*, entry assays were performed as in *A*. Cells were lysed, and HAZV-N expression was assessed by Western blot analysis. GAPDH was used as a control to confirm equal protein loading. *D*, densitometry analysis of *C*. Band densities were normalized to no-drug cells (*black columns*; $n = 3$) and compared with MTS cell viability data (*gray columns*). *, $p < 0.05$. *E*, HAZV entry assays in the presence of PF-429242. Cells were pretreated with 5–20 μM PF-429242 for 24 h and infected with HAZV (m.o.i. 0.2). Cells were lysed at 24 hpi and screened for HAZV-N and GAPDH as in *C*. *F*, densitometry analysis of *E* as in *D*. *, $p < 0.05$. *G*, entry assays performed as in *E* with U-18666A at 2.5–10 μM. *H*, densitometry analysis of *G* as in *D*. *, $p < 0.05$. *I*, HAZV entry assays were performed in the presence of simvastatin. Cells were pretreated with 10–50 μM simvastatin for 24 h and infected with HAZV (m.o.i. 0.2). Cells were lysed and screened for HAZV-N and GAPDH as in *C*. *J*, densitometry analysis of *I* as in *D*. *, $p < 0.05$. *K*, cells were pretreated with MβCD for 1 h. Simultaneously, HAZV virions were treated with buffers (pH 7.35), with or without 140 mM KCl, for 2 h at 37 °C. The buffers were diluted into 2 ml of DMEM and immediately added to A549 cells. Cells were lysed at 18 hpi and immunoblotted for HAZV-N as in Fig. 1*C*. *L*, densitometry analysis of *K* as in Fig. 1*D* (*H*). *, $p < 0.05$.

our findings are consistent with cholesterol disrupting K^+ accumulation in endosomes, which consequently hinders activation of the fusion machinery in the appropriate endosomal compartment. One possible mechanism by which this may occur is that the cellular channels responsible for endosomal K^+ accumulation require cholesterol-containing membrane
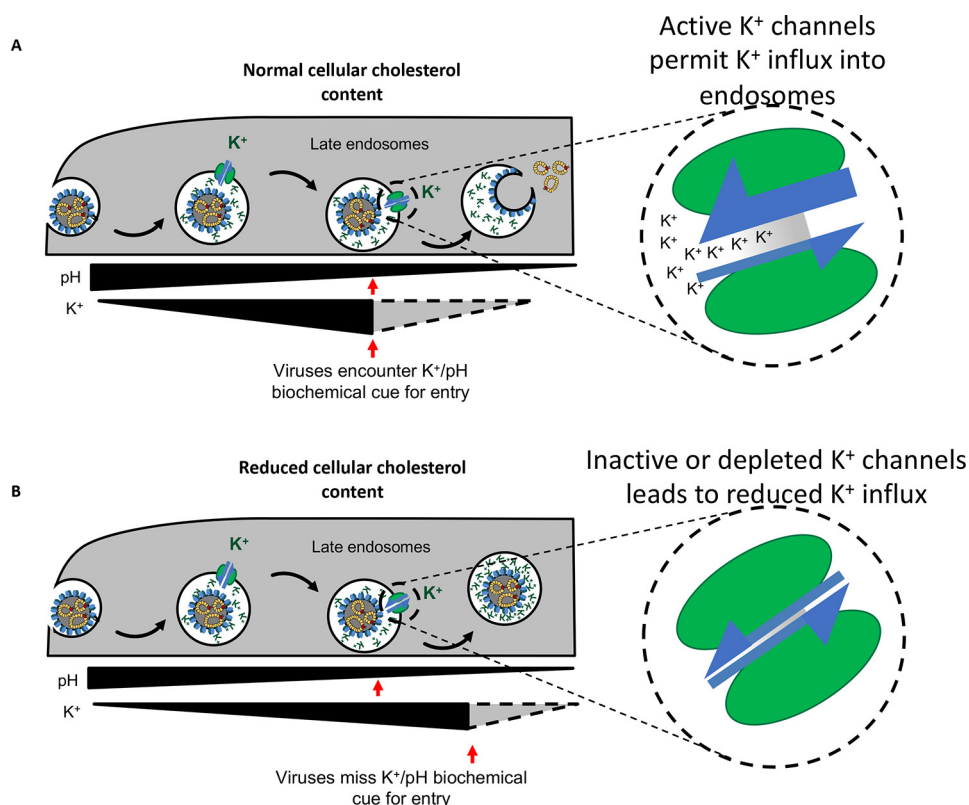
Figure 6. Cholesterol depletion may perturb K⁺ accumulation in endosomes, preventing virus escape. A putative model for the potential role of cholesterol in the accumulation of endosomal K⁺ ions. *A*, endosomal pH and the K⁺ gradient provides the biochemical cue for virus fusion and endosomal escape. This process is likely to be mediated by endosomal K⁺ channels. *B*, cholesterol depletion may inactivate or impair the function of the K⁺ channel(s) in endosomal membranes, slowing or preventing K⁺ influx into BUNV-containing endosomes. Therefore, BUNV is able to penetrate cells and to be internalized into endosomes, but the K⁺ cue is inhibited, impairing endosomal escape and subsequent virus infection.

subdomains either for their full activity or, alternatively, for incorporation into their native endosomal targets. Therefore, channels residing in endosomal membranes depleted of cholesterol may show impaired activity, thus slowing or preventing K⁺ influx into endosomes, inhibiting the K⁺ cue for endosomal escape (Fig. 6). Interestingly, cholesterol can influence K⁺ channel functionality and has been found in association with the two-pore domain K⁺ (K_{2P}) channels, acting as a linker between the central cavities of these channels and the plasma membrane core (34). Work is in progress in our laboratory to identify the specific cellular K⁺ channel(s) involved in endosomal K⁺ accumulation, and current evidence derived from an extensive pharmacological screen of blocking agents indicates that it is a member of the abovementioned K_{2P} channel family. When this information is confirmed, we will be able to further our findings in this work by examining how cholesterol influences the distribution or activity of the K_{2P} channel involved.

Although our findings reported here represent the first identification of a cholesterol requirement for infection by members of either the Peribunyaviridae or Nairoviridae families, a previous study revealed that replication of ANDV, a pathogenic hantavirus of the Bunyavirales order, was blocked when the major cellular sterol pathway was dysregulated by either genetic or pharmacological means (20). Critical genes involved included SREBP2, S1P, S2P, and SCAP, and gene ablation or knockdown studies using a nonreplicating recombinant vesicular stomatitis virus pseudotyped with ANDV-G revealed a

block in an undetermined stage of entry. The sterol pathway requirement was extended to infectious ANDV, and treatment of cells with a statin (mevastatin), a clinically approved cholesterol-lowering drug, reduced infection by more than 10-fold. Despite the fundamental differences between hantaviruses, peribunyaviruses, and nairoviruses that have led to their taxonomic separation, the possibility that infection and disease caused by highly pathogenic bunyaviruses may be treated or prevented by treatment with existing drugs is an exciting prospect.

Experimental procedures

Cells and viruses

A549 (lung epithelial carcinoma) and SW13 (human adrenal carcinoma) cells were obtained from the European Collection of Cell Cultures. A549 and SW13 cells were maintained in a humidified incubator at 37 °C with 5% CO_2 and cultured in DMEM (Sigma-Aldrich) with 10% FCS, 100 units/ml penicillin, and 100 μg/ml streptomycin (1% pen/strep). For the experiments detailed below, unless otherwise specified, A549 and SW13 cells were seeded into 6-well ($\sim$0.3 $\times$ 10⁶ cells/well) or 12-well plates ($\sim$0.1 $\times$ 10⁶ cells/well) and incubated at 37 °C for 24 h to allow cell adherence prior to each experiment.

WT BUNV and HAZV stocks were made from clarified baby hamster kidney (BHK) cell supernatants and stored at −80 °C suspended in DMEM and 10% FCS. Titers were estimated by

plaque assay, yielding ~3.5 × 10^6 pfu/ml and ~7 × 10^6 pfu/ml for BUNV and HAZV, respectively.

SYTO82/DiD-labeled BUNV was produced as described previously (16), where the three RNA segments were labeled using a SYTO82 nucleic acid stain, the viral lipid envelope was labeled using a DiD-vybrant lipid label, and the virions were purified. Recombinant BUNV, in which enhanced GFP is fused to the N terminus of truncated G$_c$ (BUNV-GFP), was kindly provided by Xiaohong Shi (CVR Glasgow).

TCEP assays

Stock solutions of TCEP (Sigma-Aldrich) were made to 1 M in deionized sterile water and frozen at −20 °C. These stocks were diluted to 10 mM in Opti-MEM reduced serum medium (Gibco) prior to each experiment. A549 cells were infected with BUNV or HAZV (m.o.i. 0.2, $t = 0$) and incubated at 37 °C. Cells were washed in PBS, and 10 mM TCEP was added for 5 min at the indicated time points, 0.5–120 min after infection. Cells were washed in PBS following TCEP treatments and incubated at 37 °C in DMEM. Cells were lysed or fixed at 24 hpi and immunoblotted or immunostained (see below) for IncuCyte Zoom® analysis of viral N protein.

MβCD entry assays

A549 cells were washed with PBS and, preinfection, treated with 2 mM, 1 mM, or 0.5 mM MβCD (Sigma-Aldrich) for 45 min at 37 °C. Cells were washed with PBS to remove the drug and infected with BUNV or HAZV (m.o.i. 0.2) for 2 h to allow virus entry. The medium and noninternalized virions were removed via one PBS wash and three 0.5% trypsin washes (2 hpi) and replaced with complete DMEM. Infection was allowed to proceed until 24 hpi, followed by lysis or fixation for Western blotting or IncuCyte Zoom® analysis.

Simvastatin, PF-429242, and U18666A entry assays

A549 cells were treated with simvastatin (Sigma-Aldrich; 10, 20, 25, or 50 μM), PF-429242 (Sigma-Aldrich; 20, 10, or 5 μM), or U-18666A (Abcam; 10, 5, or 2.5 μM) for 24 h. Cells were subsequently infected with BUNV or HAZV (m.o.i. 0.2) for 24 h, with the drug(s) maintained throughout. At 24 hpi, cells were lysed for analysis.

SYTO82/DiD-labeled BUNV infection of MβCD-treated cells

A549 cells were seeded onto 1-cm^2 glass-bottom 8-well microslides (Ibidi). Cells were treated with 2 mM MβCD for 45 min, the drug was washed off with PBS, and cells were infected with SYTO82/DiD-labeled BUNV (m.o.i. ~8) for 30 min at 4 °C to allow virus binding. This was followed by warming to 37 °C to allow synchronized entry and incubation for 8 h. 30 min prior to imaging, cells were stained with CytoPainter organelle stain (Abcam) for 30 min. Cells were washed with PBS and live-imaged by confocal microscopy in fresh DMEM.

MβCD and NH₄Cl time-of-addition assays

A549 cells (8 wells total) were infected with BUNV (m.o.i. 0.1, $t = 0$), with one well pretreated (0 hpi time point) with MβCD (2 mM) or NH₄Cl (10 mM) (Sigma-Aldrich) for 45 min prior to infection. At 1 hpi, noninternalized virus was washed off, and

medium or drug was added to the corresponding wells. MβCD or NH₄Cl was added to cells at the indicated time points, 1–10 hpi. Infection was allowed to proceed until 24 hpi, followed by lysis and assessment of BUNV infection by Western blot detection of BUNV-N.

Viral envelope cholesterol depletion

HAZV or BUNV-GFP virions were treated with MβCD (2 mM) for 90 min at 37 °C. MβCD was diluted into complete medium, and A549 cells were subsequently infected with treated virions (m.o.i. 0.5) for 24 h. Cells were fixed or lysed for detection of HAZV-N/GFP by immunofluorescent staining (IncuCyte Zoom®) or HAZV-N/BUNV-N by Western blotting.

Visualization of MβCD-treated BUNV by negative staining

BUNV was collected from BHK-21 supernatants, purified through 30% sucrose, and resuspended overnight in 0.1× PBS. Purified BUNV virions (1.5 × 10^9 pfu/ml) were treated with 2 mM MβCD for 90 min at 37 °C. Preparations were added to glow-discharged carbon-coated grids and allowed to stand for 1 min. Grids were washed three times with distilled H$_2$O and stained for 1 min with 1% aqueous uranyl acetate. Preparations were allowed to dry and imaged using a FEI Tecnai T12 electron microscope at 120 kV. Images were collected at a nominal defocus between −1 and −5 μm using a Gatan Ultrascan 4000 charge coupled device camera.

BUNV/HAZV priming recovery assays

BUNV virions (12 μl, m.o.i. 0.1) were diluted 1:11 in buffers mimicking the change in endosomal pH (pH 7.35 or 6.35) and K$^+$ concentration (0 or 140 mM KCl) and incubated for 2 h at 37 °C. Buffers were diluted out into 2 ml of fresh DMEM prior to addition to cells and added immediately to A549 cells. For the MβCD (2 mM)–treated samples, cells were treated for 1 h prior to infection (during virus priming) or left untreated, and the drug was removed from wells prior to infection. Cells were incubated until 18 hpi and lysed. HAZV virions (24 μl, m.o.i. 0.1) were diluted 1:11 in buffers mimicking early endosomal compartments (pH 7.35) with or without 140 mM KCl and incubated as above. A549 cells were treated with 2 mM MβCD for 1 h during priming or left untreated to mirror the conditions used in the BUNV assays and infected with HAZV/buffer in 2 ml of fresh DMEM for 18 h prior to lysis and screening for HAZV-N.

pH/ion buffer preparation

A buffer (pH 7.35) was used as a control alongside other buffers (pH 6.35) with a high or low K$^+$ concentration, prepared with 0.2 M Tris (pH 7.35) or 0.3 M BisTris (pH 6.35). The desired salt concentrations were achieved by adding 12 mM NaCl and ± 140 mM KCl. On the day of use, buffers were adjusted to the desired temperature and pH using 30% HCl.

K$^+$ uptake assays

A549 cells were treated preinfection with 2 mM MβCD in Opti-MEM for 45 min at 37 °C or left untreated as a control. Cells were simultaneously treated with 10 μM membrane-impermeable AG4 and 2 μg/ml Alexa Fluor– conjugated Trans-

§ASBMB

J. Biol. Chem. (2019) 294(18) 7335–7347   **7345**

ferrin-594 for 45 min, with MβCD in the medium throughout. Cells were washed in PBS and live-imaged using the IncuCyte Zoom® system.

MTS cell viability assays

A549 cells were seeded into 96-well tissue culture plates (0.05×10^6 cells/well) and allowed to grow to 70–80% confluency. Cells were then treated with the respective drugs alongside an untreated and H$_2$O-treated control for 24 h, the maximum time these drugs were applied. Cells were then screened for viability using CellTiter 96® reagent (Promega); 20 μl was added to serum-free medium for 1 h following the manufacturer's instructions. Viability was analyzed by reading absorbance at 570 nm using a plate reader. Results were normalized to the untreated control.

Western blot analysis

At the stated time points, cells were lysed in Leeds lysis buffer (25 mM glycerol phosphate, 20 mM Tris, 150 mM NaCl, 1 mM EDTA, 1% Triton X-100, 10% glycerol, 50 mM NaF, and 5 mM Na$_4$O$_7$P$_2$ (pH 7.4)) plus protease inhibitor mixture (Thermo Scientific) for 15 min at 4 °C. Lysates were resolved on 12% or 15% SDS gels using SDS-PAGE. Protein was transferred onto PVDF membranes (Millipore) using a Bio-Rad Trans-blot Turbo. Membranes were blocked in 10% milk in TBS-Tween for 1 h. Proteins were labeled with primary antibodies in 5% milk in TBS-Tween for 1 h at room temperature and then with the corresponding HRP-conjugated secondary antibodies in 5% milk/TBS-Tween. Labeled proteins were detected by ECL, and the film was developed using an Xograph processor. Quantification of bands was performed using densitometry in ImageJ software.

BUNV/HAZV was detected using BUNV-N/HAZV-N primary antibodies and corresponding anti-sheep secondary antibodies (1:5000). Anti-GAPDH antibodies were used as a loading control alongside anti-mouse secondary antibodies (1:5000).

Immunofluorescence staining

Confocal analysis—Cells were live-imaged using an inverted LSM-880 confocal microscope (Zeiss) on an oil immersion $\times$63 objective lens to image fluorescent labeling: SYTO82 (emission$_{max}$ = 560 nm), DiDvbt (emission$_{max}$ = 665 nm), and conjugated transferrin-488 (emission$_{max}$ 518 nm).

IncuCyte analysis—At the indicated time points, cells were fixed in 4% paraformaldehyde for 10 min at 4 °C. Cells were washed with PBS and permeabilized with cold 50% methanol/acetone for 10 min at 4 °C. Nonspecific antibody binding was then blocked with 1% BSA in PBS at room temperature for 15 min. Primary anti-BUNV-N or HAZV-N antibodies were added (1:5000) in 1% BSA for 1 h, followed by four PBS washes. Corresponding fluorescent Alexa Fluor 594–conjugated anti-sheep (Invitrogen/Molecular Probes) secondary antibodies (1:500) were added for 2 h in 1% BSA, followed by four washes in PBS. For K$^+$ uptake assays (2.2.8), cells were live-imaged without fixing of the staining protocols outlined above.

Cells were imaged using the IncuCyte Zoom® system, widefield images of 2.15 mm^2 were taken, and fluorescently labeled infected cells could be identified. The mean fluorescence count per well was quantified for treated cells using the IncuCyte Zoom® 2018 software, and the results were normalized to those of untreated cells.

Note added in proof—Fig. 4F contained an inadvertently duplicated image in the version of this article published as a Paper in Press on February 25, 2019. This error has now been corrected and does not affect the results or conclusions of this work.

References

1. Wolf, Y., Krupovic, M., Zhang Y Z, Maes, P., Dolja, V., Koonin E V, Kuhn, J. (2018) Megataxonomy of negative-sense RNA viruses. *Int. Comm. Taxon. Viruses* [online] https://talk.ictvonline.org/taxonomy/ (accessed January 17, 2019)
2. Soldan, S. S., and González-Scarano, F. (2005) Emerging infectious diseases: the Bunyaviridae. *J. Neurovirol.* **11,** 412–423 CrossRef Medline
3. Elliott, R. M. (1997) Emerging viruses: the Bunyaviridae. *Mol. Med.* **3,** 572–577 CrossRef Medline
4. Simons, J. F., Hellman, U., and Pettersson, R. F. (1990) Uukuniemi virus S RNA segment: ambisense coding strategy, packaging of complementary strands into virions, and homology to members of the genus Phlebovirus. *J. Virol.* **64,** 247–255 Medline
5. Fuller, F., Bhown, A. S., and Bishop, D. H. (1983) Bunyavirus nucleoprotein, N, and a non-structural protein, NSS, are coded by overlapping reading frames in the S RNA. *J. Gen. Virol.* **64,** 1705–1714 CrossRef Medline
6. Vera-Otarola, J., Solis, L., Soto-Rifo, R., Ricci, E. P., Pino, K., Tischler, N. D., Ohlmann, T., Darlix, J.-L., and López-Lastra, M. (2012) The Andes Hantavirus NSs protein is expressed from the viral small mRNA by a leaky scanning mechanism. 10.1128/JVI.06223-11
7. Simon, M., Johansson, C., and Mirazimi, A. (2009) Crimean-Congo hemorrhagic fever virus entry and replication is clathrin-, pH- and cholesterol-dependent. *J. Gen. Virol.* **90,** 210–215 CrossRef Medline
8. Jin, M., Park, J., Lee, S., Park, B., Shin, J., Song, K.-J., Ahn, T.-I., Hwang, S.-Y., Ahn, B.-Y., and Ahn, K. (2002) Hantaan virus enters cells by clathrin-dependent receptor-mediated endocytosis. *Virology* **294,** 60–69 CrossRef Medline
9. Hollidge, B. S., Nedelsky, N. B., Salzano, M.-V., Fraser, J. W., González-Scarano, F., and Soldan, S. S. (2012) Orthobunyavirus entry into neurons and other mammalian cells occurs via clathrin-mediated endocytosis and requires trafficking into early endosomes. *J. Virol.* **86,** 7988–8001 CrossRef Medline
10. Lozach, P.-Y., Mancini, R., Bitto, D., Meier, R., Oestereich, L., Overby, A. K., Pettersson, R. F., and Helenius, A. (2010) Entry of bunyaviruses into mammalian cells. *Cell Host Microbe* **7,** 488–499 CrossRef Medline
11. Garry, C. E., and Garry, R. F. (2004) Proteomics computational analyses suggest that the carboxyl terminal glycoproteins of bunyaviruses are class II viral fusion protein (β-penetrenes). *Theor. Biol. Med. Model.* **1,** 10 CrossRef Medline
12. Kuhn, R. J., Zhang, W., Rossmann, M. G., Pletnev, S. V., Corver, J., Lenches, E., Jones, C. T., Mukhopadhyay, S., Chipman, P. R., Strauss, E. G., Baker, T. S., and Strauss, J. H. (2002) Structure of dengue virus: implica-

tions for flavivirus organization, maturation, and fusion. *Cell* **108,** 717–725 CrossRef Medline

13. von Bonsdorff, C. H., and Pettersson, R. (1975) Surface structure of Uukuniemi virus. *J. Virol.* **16,** 1296–1307 Medline

14. von Bonsdorff, C. H., and Harrison, S. C. (1975) Sindbis virus glycoproteins form a regular icosahedral surface lattice. *J. Virol.* **16,** 141–145 Medline

15. Harrison, S. C. (2015) Viral membrane fusion. *Virology* **479-480,** 498–507

16. Hover, S., Foster, B., Fontana, J., Kohl, A., Goldstein, S. A. N., Barr, J. N., and Mankouri, J. (2018) Bunyavirus requirement for endosomal K⁺ reveals new roles of cellular ion channels during infection. *PLoS Pathog.* **14,** e1006845 CrossRef Medline

17. Punch, E. K., Hover, S., Blest, H. T. W., Fuller, J., Hewson, R., Fontana, J., Mankouri, J., and Barr, J. N. (2018) Potassium is a trigger for conformational change in the fusion spike of an enveloped RNA virus. *J. Biol. Chem.* **293,** 9937–9944 CrossRef Medline

18. Song, Y., Kenworthy, A. K., and Sanders, C. R. (2014) Cholesterol as a co-solvent and a ligand for membrane proteins. *Protein Sci.* **23,** 1–22 CrossRef Medline

19. Phalen, T., and Kielian, M. (1991) Cholesterol is required for infection by Semliki Forest virus. *J. Cell Biol.* **112,** 615–623 CrossRef Medline

20. Kleinfelter, L. M., Jangra, R. K., Jae, L. T., Herbert, A. S., Mittler, E., Stiles, K. M., Wirchnianski, A. S., Kielian, M., Brummelkamp, T. R., Dye, J. M., and Chandran, K. (2015) Haploid genetic screen reveals a profound and direct dependence on cholesterol for Hantavirus membrane fusion. *MBio.* **6,** e00801 Medline

21. Chlanda, P., Mekhedov, E., Waters, H., Schwartz, C. L., Fischer, E. R., Ryham, R. J., Cohen, F. S., Blank, P. S., and Zimmerberg, J. (2016) The hemifusion structure induced by influenza virus haemagglutinin is determined by physical properties of the target membranes. *Nat. Microbiol.* **1,** 16050 CrossRef Medline

22. Bajimaya, S., Frankl, T., Hayashi, T., and Takimoto, T. (2017) Cholesterol is required for stability and infectivity of influenza A and respiratory syncytial viruses. *Virology* **510,** 234–241 CrossRef Medline

23. White, J. M., and Whittaker, G. R. (2016) Fusion of enveloped viruses in endosomes. *Traffic* **17,** 593–614 CrossRef Medline

24. Cooper, R. A. (1978) Influence of increased membrane cholesterol on membrane fluidity and cell function in human red blood cells. *J. Supramol. Struct.* **8,** 413–430 CrossRef Medline

25. Hawkins, J. L., Robbins, M. D., Warren, L. C., Xia, D., Petras, S. F., Valentine, J. J., Varghese, A. H., Wang, I.-K., Subashi, T. A., Shelly, L. D., Hay, B. A., Landschulz, K. T., Geoghegan, K. F., and Harwood, H. J., Jr. (2008) Pharmacologic inhibition of site 1 protease activity inhibits sterol regulatory element-binding protein processing and reduces lipogenic enzyme gene expression and lipid synthesis in cultured cells and experimental animals. *J. Pharmacol. Exp. Ther.* **326,** 801–808 CrossRef Medline

26. Cenedella, R. J. (2009) Cholesterol synthesis inhibitor U18666A and the role of sterol metabolism and trafficking in numerous pathophysiological processes. *Lipids* **44,** 477–487 CrossRef Medline

27. Petersen, J., Drake, M. J., Bruce, E. A., Riblett, A. M., Didigu, C. A., Wilen, C. B., Malani, N., Male, F., Lee, F.-H., Bushman, F. D., Cherry, S., Doms, R. W., Bates, P., and Briley, K., Jr. (2014) The major cellular sterol regula-

tory pathway is required for Andes virus infection. *PLoS Pathog.* **10,** e1003911 CrossRef Medline

28. Poh, M. K., Shui, G., Xie, X., Shi, P.-Y., Wenk, M. R., and Gu, F. (2012) U18666A, an intra-cellular cholesterol transport inhibitor, inhibits dengue virus entry and replication. *Antiviral Res.* **93,** 191–198 CrossRef Medline

29. Wichit, S., Hamel, R., Bernard, E., Talignani, L., Diop, F., Ferraris, P., Liegeois, F., Ekchariyawat, P., Luplertlop, N., Surasombatpattana, P., Thomas, F., Merits, A., Choumet, V., Roques, P., Yssel, H., *et al.* (2017) Imipramine inhibits Chikungunya virus replication in human skin fibroblasts through interference with intracellular cholesterol trafficking. *Sci. Rep.* **7,** 3145 CrossRef Medline

30. Côté, M., Misasi, J., Ren, T., Bruchez, A., Lee, K., Filone, C. M., Hensley, L., Li, Q., Ory, D., Chandran, K., and Cunningham, J. (2011) Small molecule inhibitors reveal Niemann-Pick C1 is essential for Ebola virus infection. *Nature* **477,** 344–348 CrossRef Medline

31. Elgner, F., Ren, H., Medvedev, R., Ploen, D., Himmelsbach, K., Boller, K., and Hildt, E. (2016) The intracellular cholesterol transport inhibitor U18666A inhibits the exosome-dependent release of mature hepatitis C virus. *J. Virol.* **90,** 11181–11196 CrossRef Medline

32. Shi, X., van Mierlo, J. T., French, A., and Elliott, R. M. (2010) Visualizing the replication cycle of Bunyamwera orthobunyavirus expressing fluorescent protein-tagged Gc glycoprotein. *J. Virol.* **84,** 8460–8469 CrossRef Medline

33. Shi, X., Goli, J., Clark, G., Brauburger, K., and Elliott, R. M. (2009) Functional analysis of the Bunyamwera orthobunyavirus G_c glycoprotein. *J. Gen. Virol.* **90,** 2483–2492 CrossRef Medline

34. Lee, A. G. (2018) A database of predicted binding sites for cholesterol on membrane proteins, deep in the membrane. *Biophys. J.* 10.1016/J.BPJ.2018.06.022

35. Sun, X., and Whittaker, G. R. (2003) Role for influenza virus envelope cholesterol in virus entry and infection. *J. Virol.* **77,** 12543–12551 CrossRef Medline

36. Hover, S., King, B., Hall, B., Loundras, E.-A., Taqi, H., Daly, J., Dallas, M., Peers, C., Schnettler, E., McKimmie, C., Kohl, A., Barr, J. N., and Mankouri, J. (2016) Modulation of potassium channels inhibits bunyavirus infection. *J. Biol. Chem.* **291,** 3411–3422 CrossRef Medline

37. Kielian, M. C., and Helenius, A. (1984) Role of cholesterol in fusion of Semliki Forest virus with membranes. *J. Virol.* **52,** 281–283 Medline

38. Pelkmans, L., and Helenius, A. (2002) Endocytosis via caveolae. *Traffic.* **3,** 311–320 CrossRef Medline

39. Pelkmans, L., Kartenbeck, J., and Helenius, A. (2001) Caveolar endocytosis of simian virus 40 reveals a new two-step vesicular-transport pathway to the ER. *Nat. Cell Biol.* **3,** 473–483 CrossRef Medline

40. Medigeshi, G. R., Hirsch, A. J., Streblow, D. N., Nikolich-Zugich, J., and Nelson, J. A. (2008) West Nile virus entry requires cholesterol-rich membrane microdomains and is independent of αvβ3 integrin. *J. Virol.* **82,** 5212–5219 CrossRef Medline

41. Hover, S., Foster, B., Barr, J. N., and Mankouri, J. (2017) Viral dependence on cellular ion channels: an emerging anti-viral target? *J. Gen. Virol.* **98,** 345–351 CrossRef Medline